

Article

Cyclic Behavior of FRP Strengthened Beam-Column Joints under Various Concrete Damage Levels

Rajai Al-Rousan ^{1,*}, Osama Nusier ¹, Khairedin Abdalla ¹, Mohammad Alhassan ^{1,2},
Emmanouil A. Vougioukas ³, Athanassios A. Stamos ³ and Nikos D. Lagaros ³

¹ Department of Civil Engineering, Jordan University of Science and Technology, Irbid 22110, Jordan

² Civil Engineering Program, Al Ain University, Al Ain 307501, United Arab Emirates

³ School of Civil Engineering, National Technical University of Athens (NTUA), 15780 Zografou, Greece

* Correspondence: rzalrousan@just.edu.jo; Tel.: +962-799-887-574

Abstract: This paper is intended to examine the efficiency of utilizing the FRP composite material with an externally bonded technique in enhancing the behavior of the damaged B-C joints and controlling their failure mode using the NLFEA approach. At first, the modeled Beam-Column joint was validated as per the previously-attained experimentally-attained results. Later, the model was widened to experiment with the impact of axial-column load and the concrete compressive strength on the reinforced and un-reinforced models with FRP. To run the experiment, there were three cases of applying the axial column load: no load applied (0%), applying 25%, applying 50%, and applying 75%, while the concrete compressive strength degradation level was (0% damage), (25% damage), and (50% damage). All models were evaluated for structural performance, considering: the failure mode, stresses distribution, and the ultimate capacities in pulling and pushing with its corresponding displacements. However, the horizontal load-displacement hysteretic loops and envelopes, stiffness degradation, displacement ductility, and energy dissipation were reported. The experimental results revealed that using FRP to externally-reinforce B-C joints improved overall cyclic performance, as the FRP caused a rise in the ultimate load capacity, horizontal displacement, ductility of displacement, and displacement energy dissipation, while it slowed down the stiffness degradation. In addition, the FRP material converted the failure mode of the region between the joint and column from brittle to ductile due to the formation of a plastic hinge only on the side of the beam when the axial column load exceeded 25%. It must be noticed that when the column's axial load is less than 25%, the ultimate capacity of axial load and resultant deflection is solely improved. However, it has been stated that increasing the column's axial loading by 25% increases the resulting stiffness degradation by 3% for undamaged joints, which further increases by 16% for each increased damage level. In contrast, the absorbed energy is increased by 170% under axial loading, increasing by 25%, which is reduced to only one-fourth under the various damage levels. Generally, the resulting observations help specialized engineers retrofit appropriate B-C joints in already-standing buildings due to their accuracy.



Citation: Al-Rousan, R.; Nusier, O.; Abdalla, K.; Alhassan, M.; Vougioukas, E.A.; Stamos, A.A.; Lagaros, N.D. Cyclic Behavior of FRP Strengthened Beam-Column Joints under Various Concrete Damage Levels. *Constr. Mater.* **2023**, *3*, 38–61. <https://doi.org/10.3390/constrmater3010004>

Received: 5 December 2022

Revised: 3 January 2023

Accepted: 9 January 2023

Published: 28 January 2023

Keywords: ANSYS; FRP layers; concrete compressive strength degradation; beam-column joints; seismic action; axial loading level



Copyright: © 2023 by the authors. Licensee MDPI, Basel, Switzerland. This article is an open access article distributed under the terms and conditions of the Creative Commons Attribution (CC BY) license (<https://creativecommons.org/licenses/by/4.0/>).

1. Introduction

Reinforced concrete (RC) constructions are subjected to deterioration due to many reasons, such as environmental reasons (weathering, reinforcement corrosion, environmental conditions, and chemical attacks) or putting more loads on the construction beyond the normal capacity of the construction, such as increasing the number of floors [1]. As a result, it has been imperative to run retrofitting and maintenance for structural elements, for example, beam elements (or girders), column elements (or piers), beam joints (B-C) joints, or slabs [2–5]. Many countries have issued obligatory instructions and regulations to

maintain already-standing RC structures to improve the structure's ultimate load capacity and ductility. Researchers have performed extensive research to develop reliable and cost-effective retrofitting techniques [6–10]. It has been found that environmental attacks degraded the structural durability of structures in marine locations, walls, and foundations [11–15]. These attacks also could: degrade the hydrated cement paste, cause concrete surface to scale and shell, cause cracks in concrete, produce steel's tensile and concrete's compressive stresses, expand the area of exposed aggregate, detach the bond between concrete and steel, in addition to severely reduce the load-carrying capacity and durability of the RC structure [16,17] and thus requires upgrading using various techniques and materials such as carbon nanotubes-reinforced concrete (CNTRC) and graphene platelets reinforced composite (GPLRC) [18,19]. It is highly recommended to use concrete mixes with plenty of pozzolanic materials and cement with high environmental resistance to protect RC constructions against environmental attacks [20,21].

Civil engineering's prime concern is to upgrade and maintain defective RC members and those under design. However, in a framed structure, where the concept of a strong beam-weak column is applied, the B-C joints could form local hinging in RC columns when subjected to seismic loads. Hence, in under-load-of-gravity RC structures, beams are usually constructed stronger than columns; as well stipulated, RC columns are weak in ductility, which greatly weakens the joint panel. However, the shortage in the non-continuous strengthening at the bottom of the beam or transversally-installed reinforcement could interpret this. In addition, the joints quickly collapse under seismic activities, resulting in a degradation in their strength and stiffness [22]. The B-C joints usually fail in the brittle mode, where the strength hierarchy's lower bound is identified. Occasionally, B-C joints' brittle failure mode degrades the ductility of framed structures, causing these structures to fall apart. Therefore, the joint panels must undergo external strengthening or repair to improve the confinement effectiveness and enhance their shear capacity [23–29].

However, Fiber Reinforced Polymer (FRP) material is widely used in strengthening and repairing due to its superior advantages over traditionally-used materials such as steel. This includes its superior strength, which its lightweight accompanies, besides having corrosion-resistant properties and high fatigue performance [30–32]. Several B-C joints' strengthening and repairing methods have been studied, including damaged concrete removal or replacement, epoxy repair, concrete jacketing, exterior steel jacketing, partial infilling/jacketing, and external maintaining/strengthening methods utilizing FRP. Each technique has its requirements: level of applicability, labor considerations, incurred costs, and building occupants. Shannag and Alhassan [33] examined B-C joints' behavior when they were jacketed with high-performance concrete reinforced with fiber, known as HPFRC of 25 mm thickness, wrapped all over the joint zone. It was found that repaired joints showed a better seismic structural behavior than the reference joints, as they showed more significant load levels, less degradation rate of stiffness, and higher energy dissipation. Furthermore, the performance of an exterior beam-column joint has been evaluated experimentally by Realfonzo et al. [34] under cyclic loading and retrofitting with FRP composites where some important aspects affected the FRP joints upgrading were highlighted, especially the FRP anchorage problem. Engindeniz et al. [35] investigated, experimentally, the techniques used to strengthen and repair B-C joints and their impact on the joints' behavior. Like the previous study, the B-C joints were jacketed with HPFRC. The results achieved were remarkable [36]. In turn, many researchers have investigated the performance of reinforced-by-fiber B-C joint models, as several of them were conducted by Bousselham [37]. Meanwhile, the performance of reinforced-with-GFRP B-C joints has been experimentally examined by El-Amoury and Ghobarah [38]. Moreover, the scholars examined the joint's performance when reinforced with steel rebar and either carbon (CFRP) or glass (GFRP) FRP composite [39]. In addition, Sasmal et al. [40] investigated the seismic maintenance of non-ductile joints, utilizing a jacket of FRP wraps with steel plates. The study results revealed that the repaired B-C joints restored their strength as well as stiffness. Furthermore, the examined joints avoided deficiency that appeared in the steel reinforcement configura-

tion, which was not ductile in the first place. Lately, Antonopoulos and Triantafillou [41] broadly investigated, experimentally, (18) B-C joint specimens in an already-standing framed structure, having no essential details. Moreover, the study concentrated on: the axial load level in columns; the existence of the joint panel's steel reinforcement, transversally and longitudinally; the FRP composite's type, shape, and quantity that existed in beams and columns, in addition to the existence of shear reinforcement for confinement purposes. Lastly, the influence of FRP laminates with the impact of textile-reinforced mortar (TRM) has been examined by Al-Salloum et al. [42], where TRM was a reinforcing material used to strengthen the B-C joints that were deficient seismically. The outcomes indicated that sufficient layers of TRM might considerably increase the deformation capacity and shear strength of joints with TRM more than those with CFRP/GFRP composites.

However, the behavior of externally beam-column joints under the effect of strengthening by different CFRP composites schemes has been evaluated using the ABAQUS program by Sinaei et al. [43]. In contrast, a combined analytical and numerical study has been carried out by Mosallam et al. [44] for the behavior of internal joints under the effect of gravity and low cyclic loading retrofitted with different types of fiber-reinforced-polymeric (FRP) composite laminates and hybrid connectors. Moreover, due to the difficulties in modeling such problems, the Vector2 program has been utilized to assess the shear behavior of joints under seismic behavior in a real structure [45]. Not many researchers adopted the FE method to experiment with the behavior of reinforced and repaired B-C joints using FRP materials [45–52]. This is because it is rather complicated to simulate the concrete's shear cracks in the externally-strengthened elements, particularly in the joint region and the damaged concrete-FRP composite bond area. Since the concrete cracking mainly causes the slippage of FRP-concrete bond, it is essential to precisely model such cracks, using FEM, to describe the strengthened/repared joints' behavior. Most studies omitted the bond-slip behavior of the bond between concrete and FRP, especially when debonding failure was simulated. There has been a good agreement between experimental and theoretically-obtained ones regarding the patterns of cracking; or distribution of strains in fiber laminates [45–53].

Reinforced concrete B-C joints risk deterioration due to external environmental attacks. That is because this type of attack degrades the joints' structural capacity. As a result, the B-C joints must be externally strengthened with high-quality composite composites, such as FRP. This strengthening method consists of confining (or wrapping) the B-C joints from the outer side by wraps of FRP. This method restores the joint's structural capacity and prevents brittle failure, which is abrupt. The NLFEM method has been used in this numerical investigation to create comprehended guidelines regarding internally strengthening concrete compressive strength degradation damaged B-C joints with FRP since the available design codes suffer a severe shortage. This is achieved considering the effectiveness of both the axial column load and the level of damage by concrete compressive strength degradation. As a result, the study has adopted the Non-Linear Finite Element Analysis (NLFEM) modeling to predict patterns of cracks and seismic behavior and the type of failure of the environmentally-damaged models that were reinforced, from the external side, with FRP. Relationships representing the concrete's mechanical characteristics were used in simulating the beam-column joint's response. Further, adequate models were devised to investigate damaged/un-damaged concrete, the reinforcing bars of steel, the bond between concrete and steel, and experimental conditions. The present experiment started with validating the model with respect to Shannag and Alhassan's outcomes [33]. After that, the validated models were expanded to investigate the behavior of unstrengthened and strengthened joints under the following sensitive parameters: the axial load of the column (0%, 25%, 50%, and 75%), and the concrete compressive strength degradation level was of (0% damage), (25% damage), and (50% damage).

2. Experimental Program Overview

In a study presented by Shannag and Alhassan [33], RC B-C joints were prepared and cured, as shown in Figure 1. The specimen’s geometry represented the inflection points between the columns and the ones between beams (i.e., null-moment points) at the column-beam mid-span location, under cyclic loading. However, steel-plate supports were fixed at the bottom side of the column, where the top side was left free to permit the column of relative drift, while the beam’s two-end were simply supported by rollers (Figure 1). In addition, the concrete of 27 MPa compressive strength was used, whereas the yielding strength of steel bars-in deformation-was 310 MPa. The column’s loads were added utilizing two hydraulic actuators with a compression capacity of 160 kN and tensile capacity of 90 kN (Figure 1). An adequate cyclic loading history was applied to simulate earthquake activity (Figure 1).

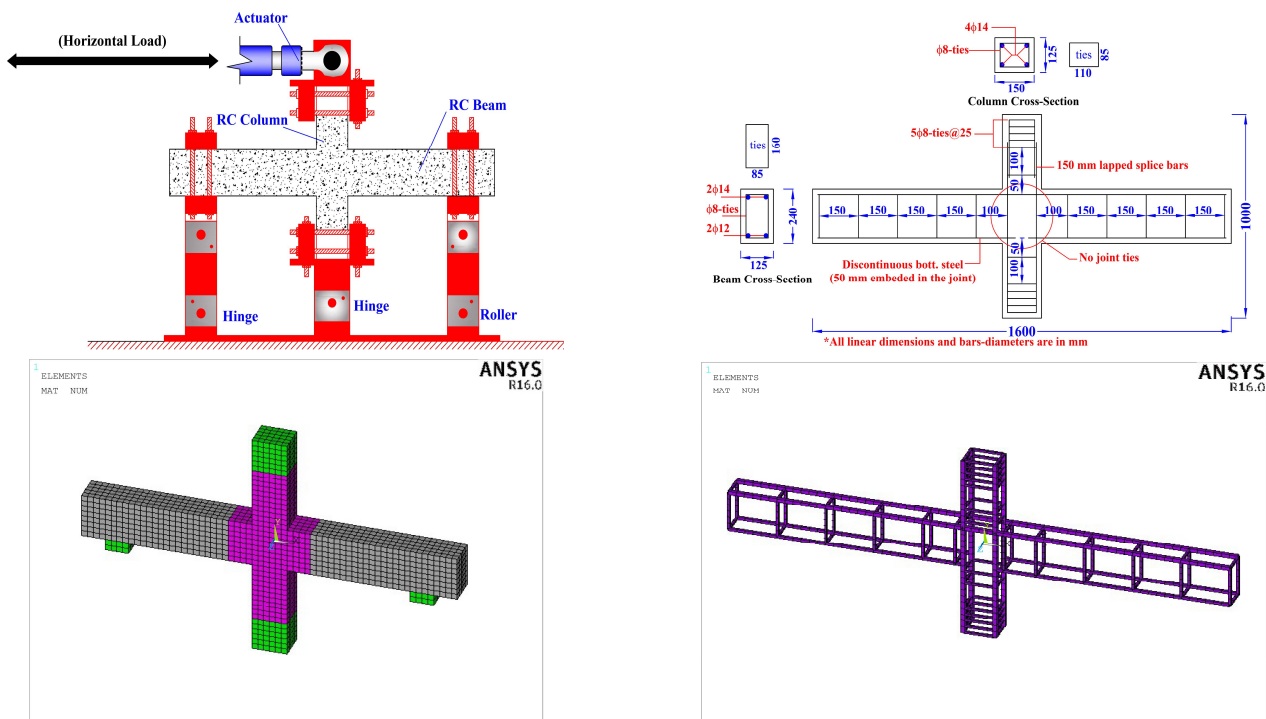


Figure 1. Testing details comparison; Experimental [33] and NLFEA [54].

3. NLFEA Description

NLFEA method is highly efficient in the simulation of RC structures, regardless of their complexity, as it saves costs, time, materials, and labor. Through highly precise simulation, the designer can reveal any design mistakes and correct them before the actual execution. Moreover, the design can be modified by adjusting any variable (loads, displacements, stresses, strains, etc.) to monitor its effect at any location and under various situations. For more accurate simulations, the ANSYS program package (a high-fidelity, 3D FEA software) [54] has been employed to predict the specimen’s seismic performance, as elaborated in Table 1. Afterward, the models were enlarged to monitor the performance of the models, with/without FRP reinforcement, was impacted by: the axial load level in the column (0%, 25%, 50%, and 75%), and the concrete compressive strength degradation level was of (0% damage), (25% damage), and (50% damage), as shown in Table 1. As per the code ACI 318-08 [55], the column’s axial load level of 0% corresponds to 0.0 kN; 25% corresponds to 63.5 kN, 50% corresponds to 127.0 kN, and 75% corresponds to 190.5 kN.

Table 1. NLFEA results of all models.

Specimens	P_u , %	FRP	f_c Damage Level	Maximum Load in Pulling, kN	Maximum Net Drift in Pulling, mm	Maximum Load in Pushing, kN	Maximum Net Drift in Pushing, mm
J0FRP0D0	0	None	0%	14.40	7.61	14.40	7.61
J25FRP0D0	25			21.60	14.85	21.60	14.85
J50FRP0D0	50			25.92	22.53	25.92	22.53
J75FRP0D0	75			27.36	26.77	27.36	26.77
J0FRP0D25	0	None	25%	10.86	5.90	10.86	5.90
J25FRP0D25	25			16.75	12.29	16.75	12.29
J50FRP0D25	50			20.29	17.20	20.29	17.20
J75FRP0D25	75			21.60	20.48	21.60	20.48
J0FRP0D50	0	None	50%	7.91	5.11	7.91	5.11
J25FRP0D50	25			12.61	9.90	12.61	9.90
J50FRP0D50	50			15.58	14.66	15.58	14.66
J75FRP0D50	75			17.55	17.65	17.55	17.65
J0FRP1D0	0	1 Layer	0%	27.82	14.81	27.82	14.81
J25FRP1D0	25			43.84	29.18	43.84	29.18
J50FRP1D0	50			55.07	38.04	55.07	38.04
J75FRP1D0	75			58.96	45.73	58.96	45.73
J0FRP1D25	0	1 Layer	25%	22.18	9.82	22.18	9.82
J25FRP1D25	25			34.56	19.75	34.56	19.75
J50FRP1D25	50			44.68	26.12	44.68	26.12
J75FRP1D25	75			49.89	32.39	49.89	32.39
J0FRP1D50	0	1 Layer	50%	16.85	7.78	16.85	7.78
J25FRP1D50	25			26.94	17.28	26.94	17.28
J50FRP1D50	50			35.21	22.91	35.21	22.91
J75FRP1D50	75			40.96	28.12	40.96	28.12

Note: P_u is the axial load.

3.1. Modelling of B-C Joint Using NLFEA

Upon constructing the modeled joints using NLFEA, the following factors have been considered: the concrete material nonlinearity (Figure 2), the elastoplastic behavior of steel reinforcement (Figure 2), added to the elastic response of FRP composites, as shown in Figure 2). Besides utilizing the ANSYS program package with elements of higher orders [54]. The procedures began with validating the simulated FE B-C joint with respect to the experimentally-achieved results of Shannag and Alhassan [28]. Next, the models were enlarged to study the effect of other variables: the axial load level and the damage extent. When preparing the models, the values of the concrete’s compressive strength were: 40, 30, and 20 MPa, while the concrete’s tensile strength was at values of: 2.6, 1.9, and 1.4 MPa, which were set at levels of (0% damage), (25% damage), and (50% damage), respectively, as illustrated in Figure 3. The models’ detailed geometry and reinforcement are demonstrated in Figure 1. The best suitable dimensions of the mesh were employed in the modeling process post carrying out the convergence test with a satisfactorily-accurate numerical solution. It was affirmed by the results obtained in a reasonable processing time [33].

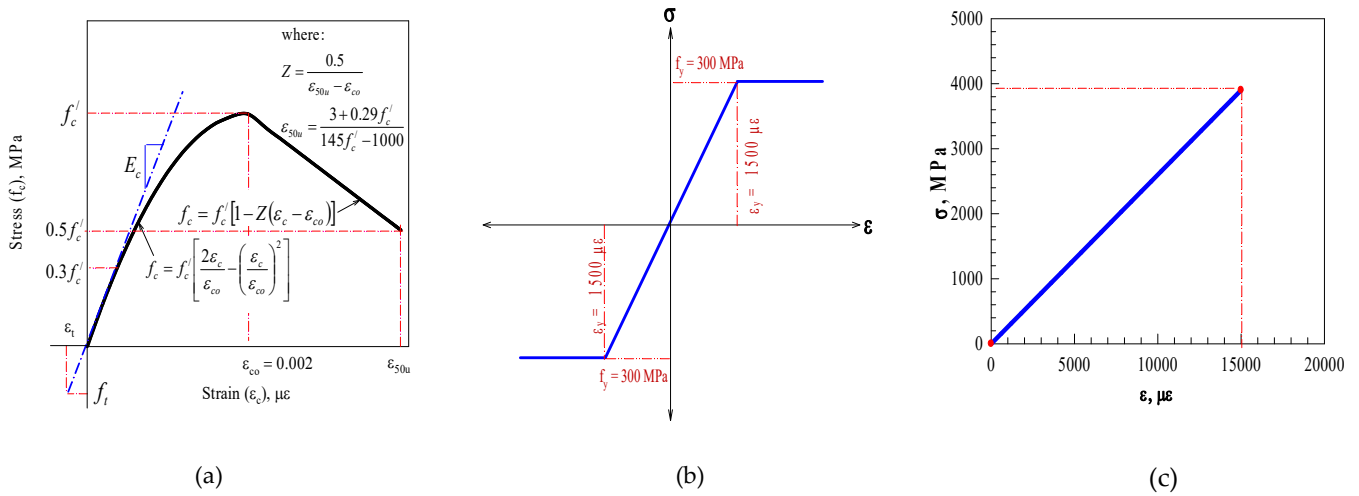


Figure 2. Material mechanical characteristics. (a) Concrete compressive strength [56], (b) Concrete tensile strength [33], (c) CFRP [57].

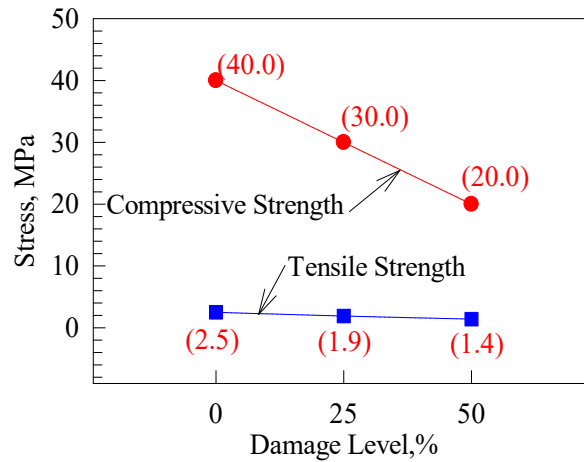


Figure 3. Concrete strength degradation.

For a more realistic simulation of B-C models, boundary conditions were set. The first boundary was to apply a hinge on the column’s bottom end and free movement at their end; the beams were also equipped with roller constraints, at the center point of supporting steel plates, on the right and the left (Figure 1). The second boundary was applying an axial load, as a first loading stage, on the column’s free edge where the cyclic loading was applied to simulate the earthquake load (Figure 1).

3.2. Material Modeling

Concrete: the concrete mix was prepared to utilize SOLID65, an eight-node solid element that can move at every node in all directions. Furthermore, Solid65 can mimic the state of crushing, the development of cracks, and plastic deformation in all directions. However, the Solid65 element can capture the crushing failure in the concrete material but has been ignored since this case has not been monitored experimentally when applying the load [45–52]. Therefore, the joint models’ tensile strains are governed by the resulting cracks and the ultimate structural element capacity [45–52]. The value of 0.2 has been selected for Poisson’s ratio for this experiment, as the usually-used value ranges between 0.15 and 0.22 [58]. The concrete elastic modulus, compressive and tensile strength have been determined to capture the resulted failure in the concrete material as depicted in (Figure 3) [59]. The shear transfer coefficient (β_t) defines the condition of the side of cracking with 0.2 [60,61]. For more precise FEM models, the stress–strain behavior of concrete has

been modeled by Kent and Park [56], who presented a descriptive model to describe the stress–strain relationship for concrete (Figure 2).

Steel: The Link180 element has been utilized to model the steel reinforcement, which can plastically deform and move freely on all sides at all nodes. The bond at the concrete–steel interface has been assumed to be perfect since the loss in the damaged concrete’s strength was negligible [62]. The reinforcing steel bars had similar tensions and compressions, with an elastic–plastic property of 200 GPa and 0.3 for the elastic modulus and Poisson’s ratio, respectively, as in Figure 2.

Steel plates: plates were modeled using SOLID45, a brick element with eight nodes capable of moving freely in every orientation. A linear elastic behavior with 200 GPa modulus of elasticity and 0.3 Poisson’s ratio has been selected for modeling the element’s behavior.

FRP composites: internal FRP laminates were modeled utilizing SOLID186, which handled up to 250 layers of FRP in many orientations. In Figure 2, the FRP laminates’ mechanical properties are illustrated. The FRP laminates were presumably elastic, linear, and orthotropic, with a 0.35 value for Poisson’s ratio [63]. The perpendicular-direction modulus of elasticity was neglected, i.e., considered a unidirectional fiber. However, the interface bond between the FRP and concrete materials was assumed to be perfect.

3.3. Data Entry and Failure Criteria

The SOLID65 element was used to capture the resulting degradation in the concrete and steel material. However, three sets of real constants were introduced that could capture the real behavior of the studied joints under various cases. Lastly, the fourth constant set included the direction and thickness of the FRP composites. However, a mesh size of 25 mm was utilized for all models, including control models, damaged models, and those strengthened with FRP. It was specified by adopting a convergence approach. In Figure 1, the joint models that have been discretized are illustrated. Hinge supports were assumed at both column ends (U_x and U_y equal to 0), while roller supports were the beams’ boundary conditions (U_y equal to 0) at the two ends of the beam. The first step of the process was to add the axial column load. Later, the horizontally-applied load was simulated as a displacement control to capture the descending part of the load–displacement curve. However, loading has been applied in substeps to avoid abrupt failure, which might cause the solution to diverge, stabilizing the analyzing procedure. As stipulated, the ANSYS software [54] discretized the applied load automatically into steps that could be entered manually, where the stiffness matrix is recalculated at the end of each step. However, the iterative Newton–Raphson equilibrium procedure with 0.001 tolerance. As the tensile and compressive stresses govern the failure criterion of concrete, the multi-linear isotropic (MISO) plasticity has been used along with Kent and Park model [56]. As stipulated, failure usually occurs if the prime compressive or tensile stresses, in all orientations, emerge out of the failure surface.

3.4. Validation

3.4.1. Control B-C Connection

Results of the horizontal load versus the net drift hysteresis loops have been plotted along with NLFEA results and compared as illustrated in Figure 4, where a significant agreement has been reached with the experimentally-obtained loops in terms of the ultimate capacity and net drift values. So, the experimental B-C joint models’ capability of reducing seismic behavior and evaluating their mechanical response is validated. However, it is observed that S8 specimens have asymmetrical hysteretic loop behavior due to the higher induced strain rate, where it undergoes a high drift value under a lower loading stage compared to other validated specimens, and this lower rate resulted in a software divergent within one cycle causing the unusual behavior appeared in S8 specimen. In detail, the following sections discuss the predictions of the damaged, strengthened-with-FRP joint model’s cyclic behavior. The generated-by-NLFEA failure modes were in big agreement

with the achieved experimentally-obtained results (Figure 5). It has been shown that the strength of the modeled joint area degraded. In contrast, the beam model showed inelasticity, with little hairline-shaped cracking. This identified mechanism is governed based on the strong column weak beam concept, which produced a pre-mature joint failure.

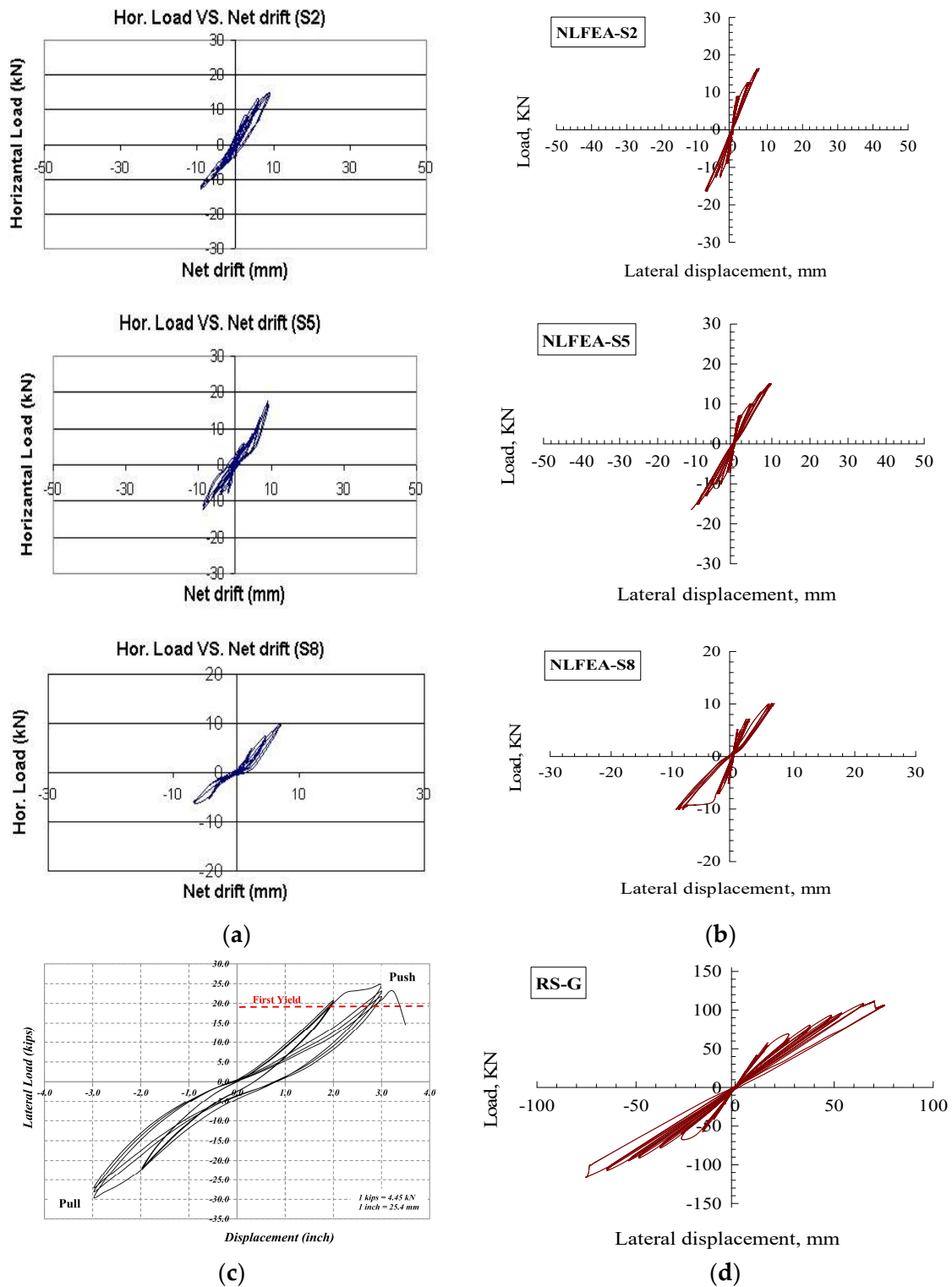


Figure 4. The hysteretic loops validation. (a) Shannag and Alhassan [33] control B-C, (b) NLFEA control B-C, (c) Khaled et al. [57] strengthened B-C, (d) NLFEA strengthened B-C.

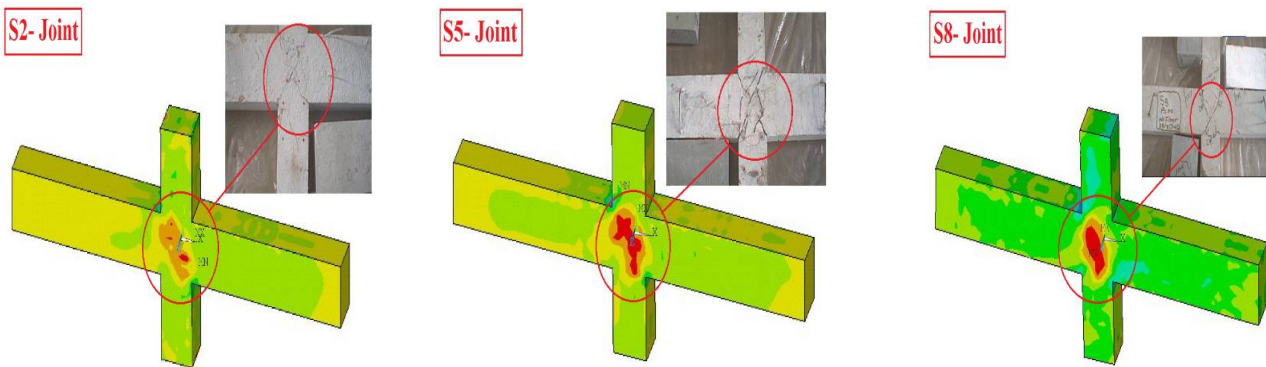


Figure 5. Failure modes validation.

3.4.2. FRP Strengthened B-C Connection

Eight full-scaled samples of interior joints between the beam and column have been tested by Khaled et al. [57] that were designed in compliance with the code (ACI 318-14) [59]. Low-frequency full-cyclic and gravity loads were applied to a sub-assembly of the samples. The beams were dimensioned as 254 mm × 406 mm. The beams were reinforced, in a longitudinal orientation, along with installing four 19 mm bars on both of the beam’s ends, at the top and bottom, and transversely strengthened with (13) mm-stirrups of steel that were evenly put at 102 mm spacing between them on the face’s center of the column located at a 381 mm distance from the edge of the beam. In contrast, the remaining were placed at a 76 mm spacing. The column has a 254 × 406 mm² cross-section and is reinforced at the top and bottom ends with four 19 mm steel, resulting in approximately 2% reinforcement ratio with a total height that is fully confined stirrups of 13 mm length, having a 76 mm spacing center-to-center. To elaborate more on the precision of NLFEA modeling of reinforced B-C joint where the load versus the drift were compared as per Figure 4b, where a good agreement was captured to an extent, with the results achieved by Khaled et al. [57] besides comparing the stress contours in Figure 6 where the resulting differences were less than 15% that could be considered an acceptable value. However, results were compared as illustrated in Table 2. In addition, Figures 4b and 6 show that NLFEA predicted, with high accuracy, the ultimate load and load-drift hysteresis response until failure. However, in this study, only the effect of utilizing one FRP layer was presented since the literature performed for validation does not examine the multi-layer FRP effect besides the resulting enhancement being good and feasible. Meanwhile, the effect of multi-layers could be further investigated after ensuring that no FRP debonding will occur between the layers.

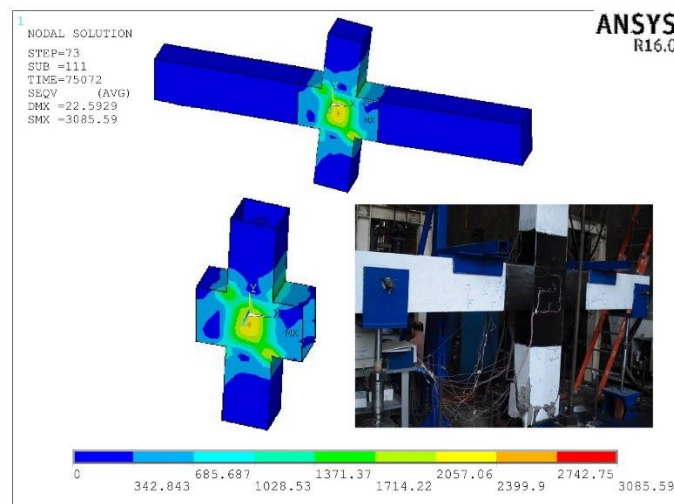


Figure 6. Stress contours validation.

Table 2. NLFEA and Tested results comparison.

Specimen	Maximum Horizontal Load, kN	Maximum Horizontal Net Drift, mm	Yield Displacement, mm	Maximum Displacement, mm	Displacement Ductility	Energy Dissipation, kN.mm
Tested Results						
S2	15.02	9.09	6.50	9.09	1.40	673
S5	16.50	9.25	6.80	9.25	1.36	843
S8	10.10	6.96	6.30	6.96	1.10	288
NLFEA Results						
S2	16.25	7.84	5.60	7.84	1.36	628
S5	16.50	10.64	7.67	10.64	1.34	950
S8	10.00	7.94	7.17	7.94	1.09	325
Error %						
S2	−8.2	13.8	13.9	13.8	2.4	6.7
S5	0.0	−15.0	−12.7	−15.0	1.8	−12.7
S8	1.0	−14.1	−13.8	−14.1	1.1	−13.0

4. Results and Discussion

4.1. Stress Contours

The theoretically-obtained stress contours of the expanded joint models are illustrated in Figure 7; specimen J25FRP1D0 is equipped with one layer of FRP as reinforcement, with an axial loading level of 25%. The control specimen had the initial diagonal cracks at the joint’s corners, at the top and bottom, in the pulling phase of loading. Generally, flexural cracks are initiated at the tension zone of the joint’s furthest fibers, around the column’s ends; later, the cracks expand flexural cracks sideways. Further, evenly-shaped cracks emerged in the pushing and pulling loading directions, along with an increment in the displacement values. Inspecting Figure 6 shows that the joint area encountered a degradation in strength, whereas the beam stayed inelastic with the emergence of some tiny cracks. This failure is called the (weak-column strong-beam) failure, which results in an abrupt failure of the joint model. Flexural cracks extend up to 650 mm from the edge of the column along the beam. Conversely, the un-reinforced (control) B-C joint witnessed flexural cracks extending across the beam to 300 mm from the column’s edge. During the pushing phase, cracks emerged in the same model but in the opposite diagonal direction. So, the control model exhibited a significant vulnerability of the joint panel zone and failed in shear. However, the joint model’s behavior maintained its elasticity without plastic hinging. Figure 7 reveals that the steel’s stress at failure was 310 MPa (matching the point of yielding). Lastly, Figure 7 shows that the stress failure of the FRP was 3086 MPa (almost 81% of stress at rupture of FRP). This indicates the effectiveness of FRP jacketing in availing better protection to the joint panel and externally strengthening the joint model. However, the presence of FRP composite in the most-critical location resulted in eliminating the resulting flexural crack and suppressing the brittle type of failure by forming a plastic hinge at the side face of the beam ending up with a ductile type of failure. So, the behavior of a strengthened-with-FRP-jacketing joint model showed improved cyclic performance as the joint panel’s failure took place in the beam. In this case, the load-carrying capacity of the joint is mainly controlled by its flexural capacity.

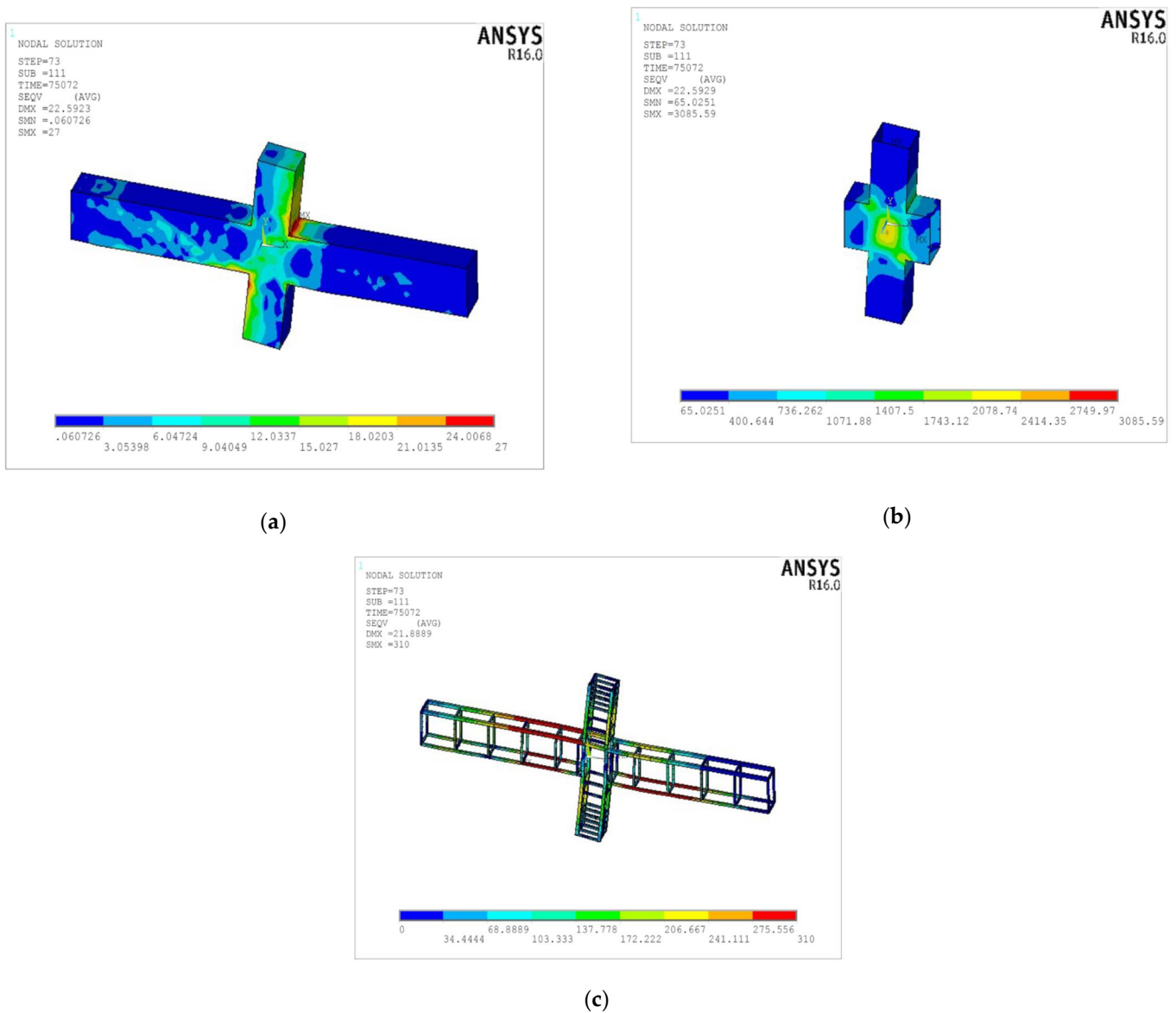


Figure 7. Stress contours for J25FRP1D0 joint (a) concrete, (b) FRP, and (c) Steel.

4.2. The Load Versus Displacement Hysteretic Loops

The load versus the horizontal displacement is plotted in Figure 8 (0% damage), Figure 9 (28% damage), and Figure 10 (50% damage). Figure 10 indicates that the un-strengthened joint with zero axial loadings modeled joint, tested at 50% damage level J0FRP0D50, experiences lower load and displacement values. In contrast, the model J0FRP0D0 (un-reinforced, no axial load, and 0% damage) (Figure 8) had the most significant strength and correspondent displacement, compared to joints J0FRP0D25 (Figure 8) and J0FRP0D50, despite the inadequately-imposed lateral reinforcement in turning the failure to occur within the beam. Horizontal load-displacement loops of the reinforced joints showed a significantly improved performance in horizontal load and correspondent displacements (Figures 8–10) because the region was confined with FRP, as it availed internal arresting mechanism of cracks besides increasing the ductility capability after cracking occurs. Moreover, the loops are also affected by the axial loading level, where the column’s compressive stress is improved under increasing the loading level (Figure 8 through Figure 10), which resulted in initiating cracking in the joint tensile concrete, causing a strength degradation. Furthermore, Figure 11 exhibits the modeled joint’s load-displacement envelopes, where the highest load and correspondent displacement values are obtained in every half-cycle

of loading (push-pull). Figure 11 revealed a proportional relationship between the axial loading level and the load displacement, but the displacement lessened when the level of damage was increased.

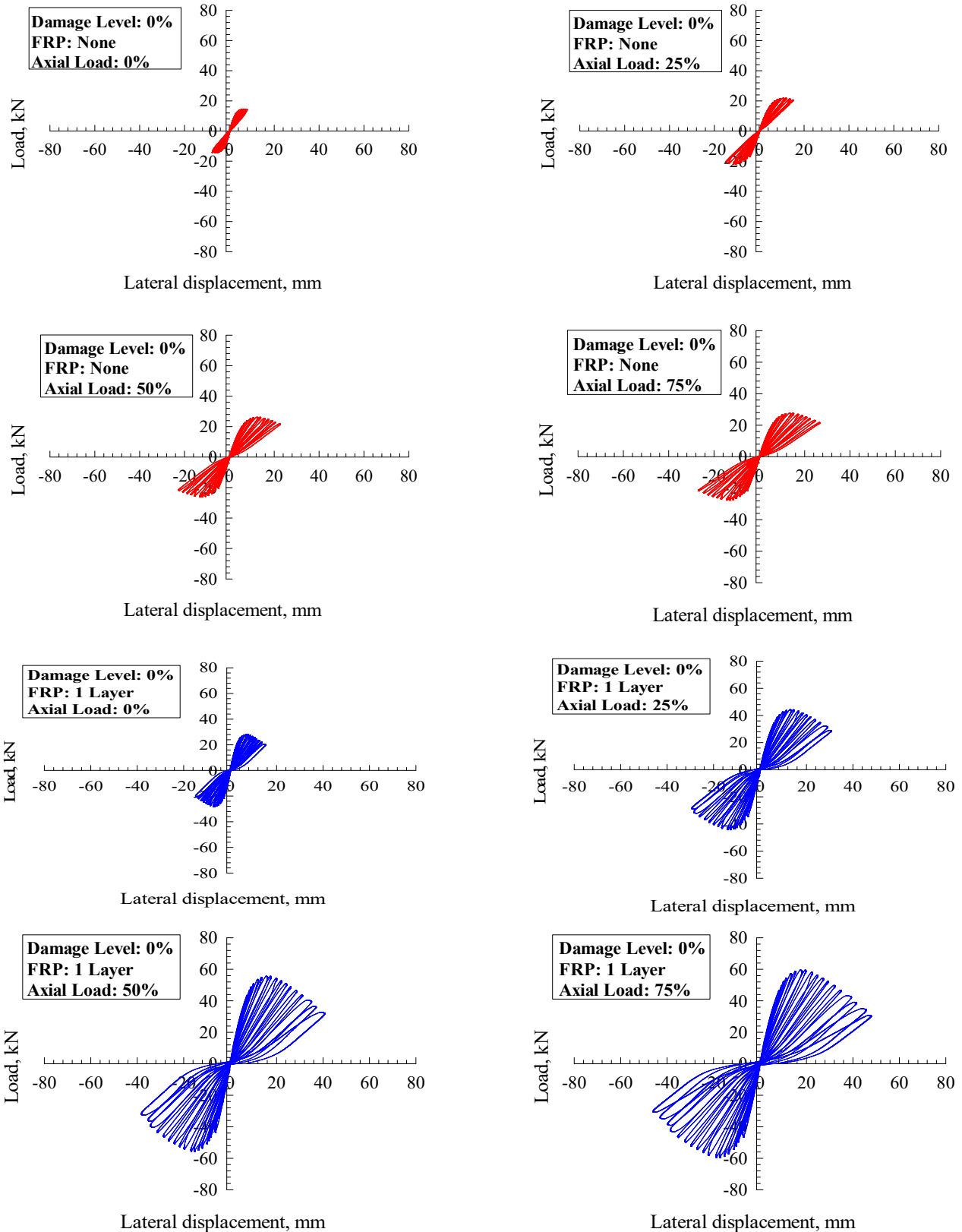


Figure 8. Hysteretic loops for undamaged joints.

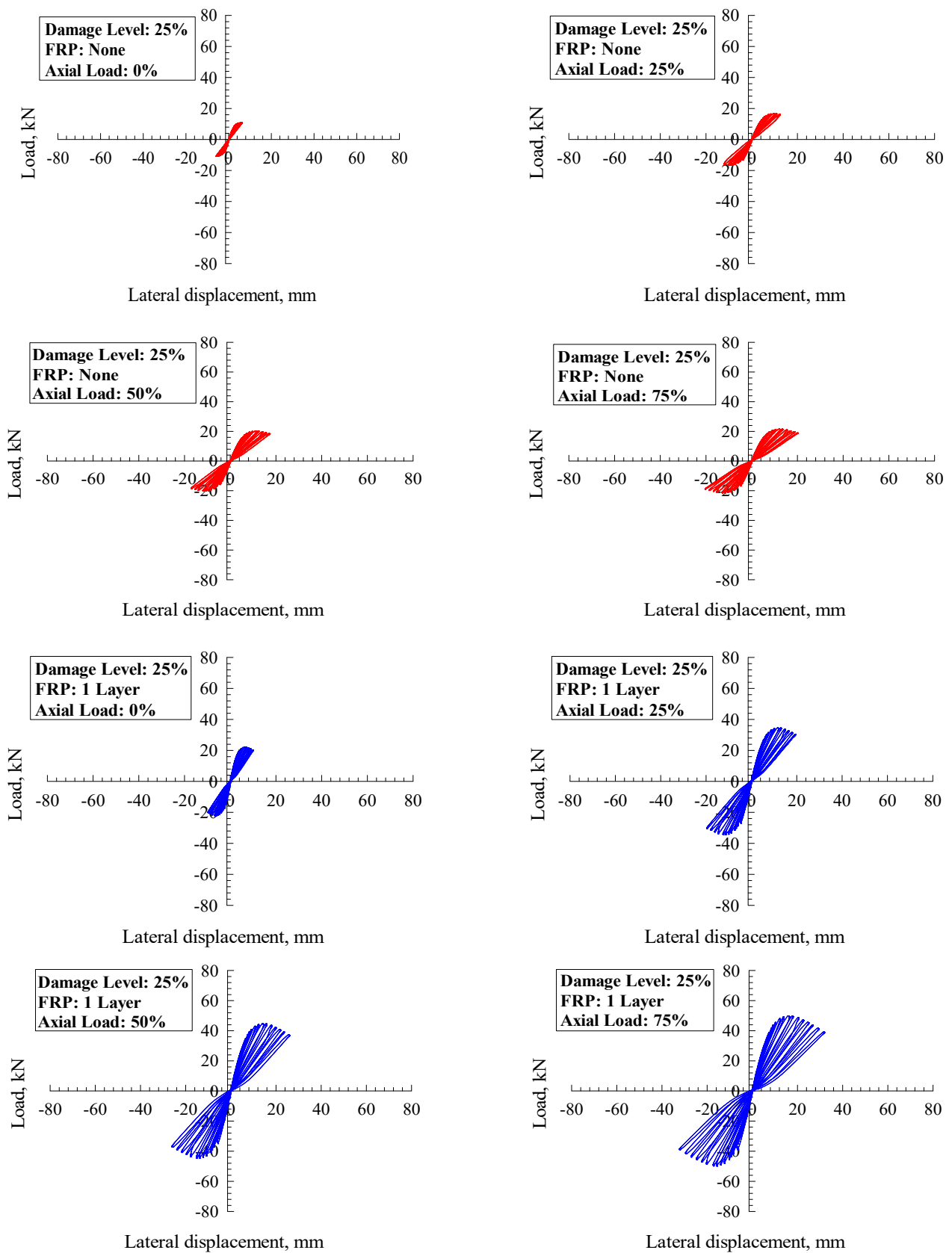


Figure 9. Hysteretic loops for 25% damaged joints.

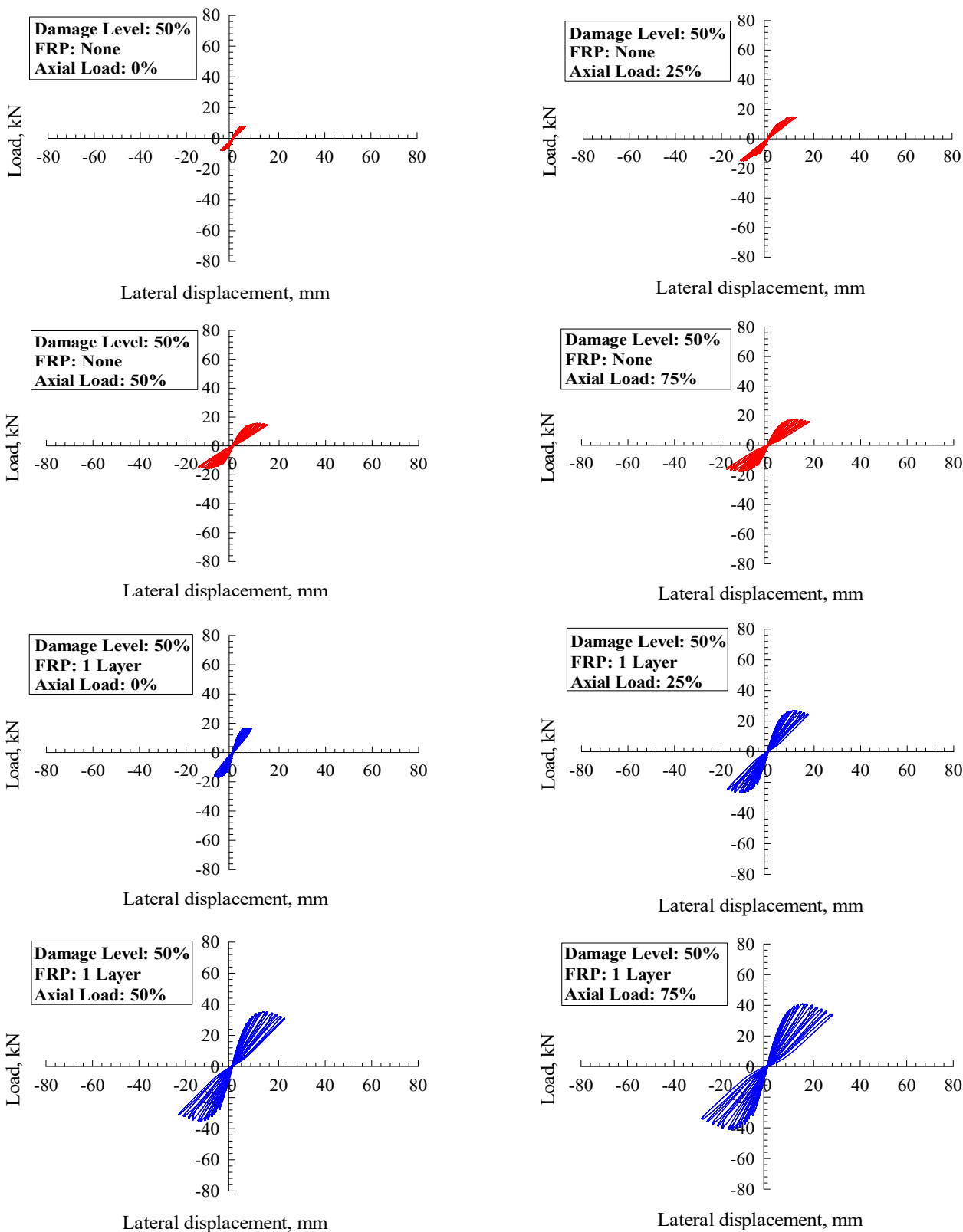


Figure 10. Hysteretic loops for 50% damaged joints.

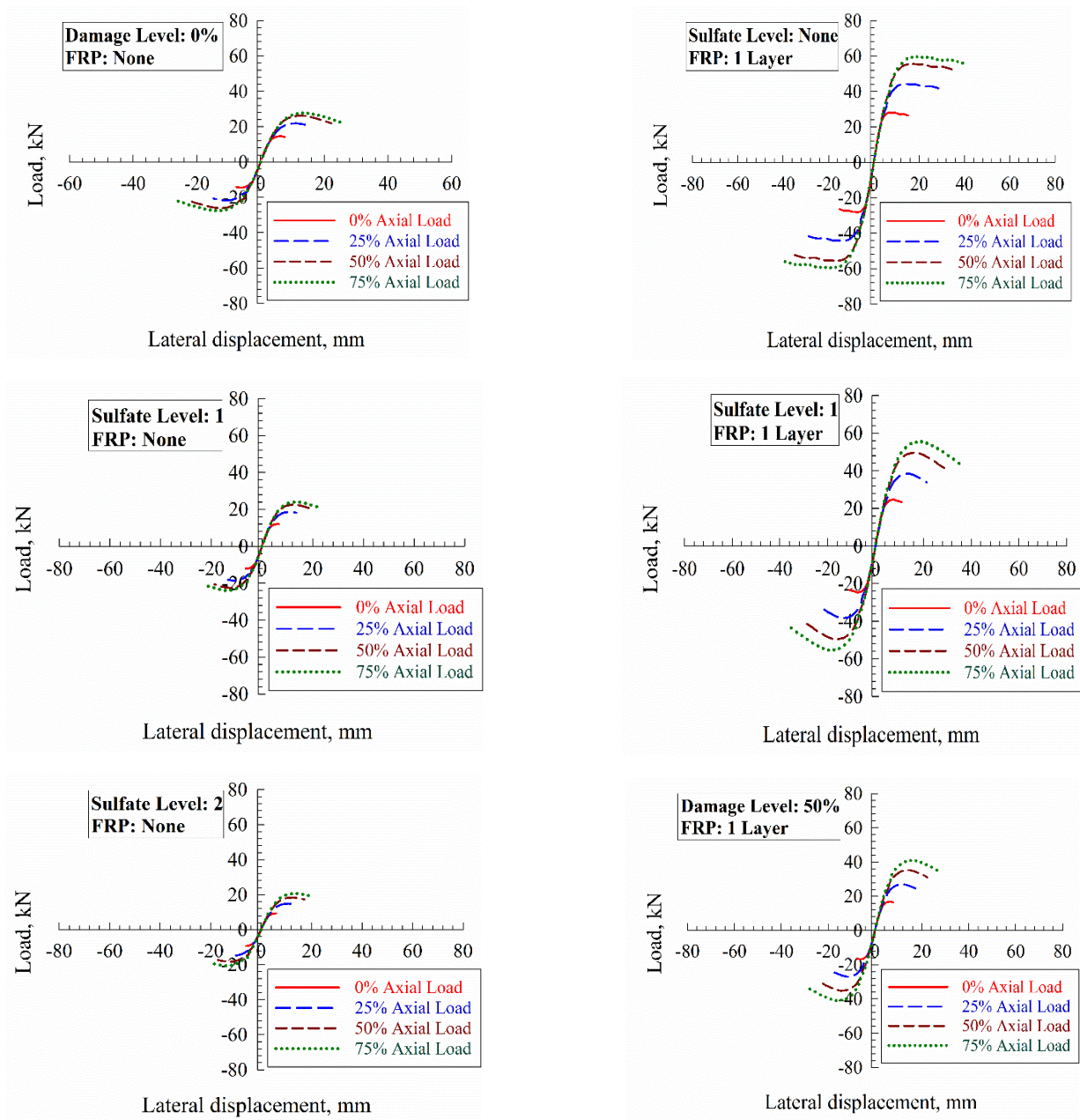


Figure 11. The load versus the lateral displacement envelopes.

Moreover, it was observed that reinforcing elements with FRP had positively influenced the horizontal loading and displacement capacities. The load was enhanced (normalized with respect to a joint with 0% axial loading) by 52%, 81%, and 89%, corresponding to axial loading levels of 25%, 50%, and 75%, respectively. On the other side, displacement was improved (normalized with respect to a joint with 0% axial loading) by 93%, 192%, and 250% under axial loads of 25%, 50%, and 75%, respectively. Furthermore, 0% damage decreased the load by 14.6% and displacement by 13.7%, at 25% damage, while 50% damage decreased the load by 30.2% and displacement by 22.9%. Further, FRP-strengthened joints have enhanced loading and displacement capacities (compared to the un-damaged joint sample): 104%, 83% at 0% damage level; 82%, 34% at 25% damage; and 52%, 23% at 50% damage.

4.3. Horizontal Displacement Versus Steel and FRP Strain Envelopes

The obtained strain data of the steel reinforcement were utilized for the modeled joints near the interface between the joint and the beam. The strain-displacement envelopes of steel rebar are graphed in Figure 12. All of the joint specimens without reinforcement (excluding J50FRP0D0, J75FRP0D0, and J75FRP0D25) fail before steel yielding occurs (Table 2), as per the B-C joint’s design criteria. It has been observed that the whole reinforced-with-FRP joints failed at the beam’s highest capacity, where the steel rebar’s tensile strain was significantly higher than the threshold of the yielding strain. Moreover, the displacement versus the strain envelopes for FRP-strengthened joints are illustrated in Figure 13. By inspecting Figure 13, it is observed that the FRP composite proved efficient as the joint’s horizontal displacement was: 8.0 mm, 6.5 mm, and 5.9 mm when the joint was exposed to damage levels of 0%, 25%, and 50%, respectively. This indicates that the concrete was negatively affected because the damage level made the FRP carry the applied load at the early stages. Furthermore, Table 2 shows that the FRP has good effectiveness by increasing the axial load by 52%, 73%, 92%, and 97% of the maximum FRP strain of 15,000 $\mu\epsilon$ corresponds to axial loading levels of 0%, 25%, 50%, and 75%, respectively. The damage level decreased the strain of FRP by 11% at a 25% damage level and 22% at a 50% damage level.

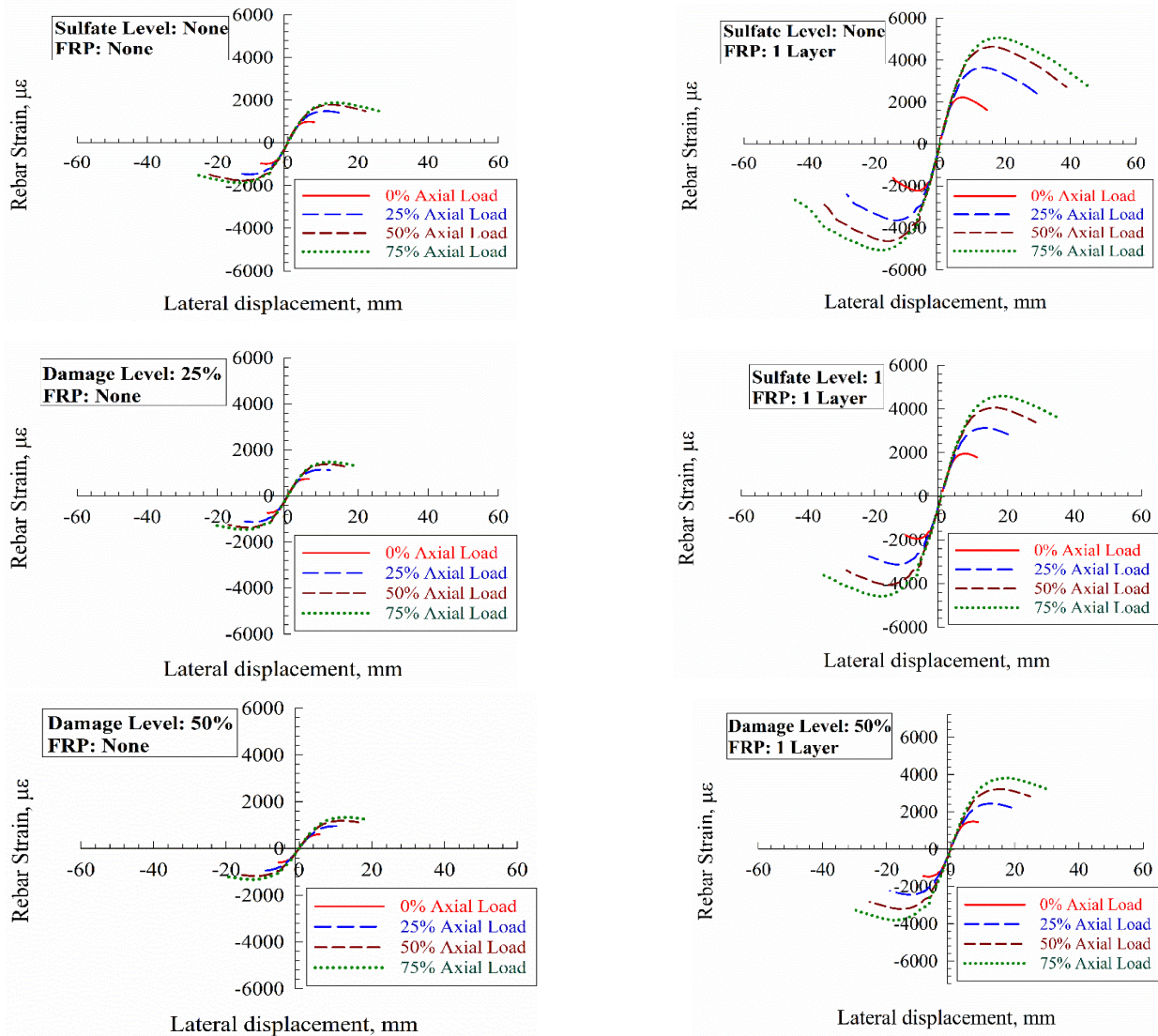


Figure 12. The beam’s reinforcement steel strains.

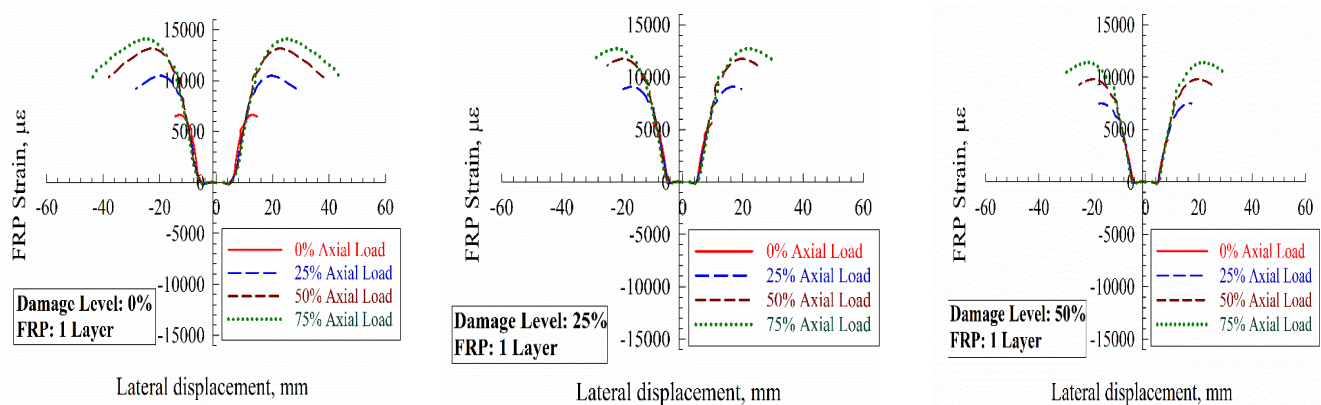


Figure 13. FRP’s strains.

4.4. Displacement Ductility and Energy Dissipation

The ratio between the ultimate and yield displacements ($\frac{dm}{dy}$) is known as the displacement ductility index. Strengthened NLFEA models’ values of displacement ductility are shown in Table 3, from which it can be seen that the displacement ductility of the models was 0, indicating a fragile seismic behavior. This does include the models: J50FRP0D0, J75FRP0D0, and J75FRP0D25. The reason behind this bad behavior is that failures occur before steel yielding is reached. However, the strengthened-with-FRP joint models showed higher values of displacement ductility (twice as much) than the un-strengthened models (i.e., J50FRP0D0, J75FRP0D0, and J75FRP0D25). This was because the strengthened models were perfectly confined with FRP wraps, which made the joints’ failure ductile where a plastic hinge is initiated within the beam element. Moreover, Table 3 shows that there was an enhancement in the displacement ductility due to applying axial load (in comparison with a strengthened joint specimen with 0% axial load) by; 95%, 185%, and 340% corresponding to axial loading levels of 25%, 50%, and 75%, respectively. Further, the ductility is reduced by 45% at 25% and 60% at 50% under the different damage levels.

Energy dissipation is an essential criterion to evaluate a B-C joint’s performance. This criterion measures the energy lost by the joint before the system de-stabilizes. B-C joints lose considerable energy due to inelastic deformation, which minimizes the amount of dissipated energy, and ensures structural safety. Energy dissipation is determined by computing the constrained area under the total load-displacement envelopes. Table 3 exhibits the energy dissipated by the joint models. The un-reinforced joint models had a fairly-low energy dissipation, as indicated by the little constrained areas under the horizontal load-displacement hysteretic loops (Figures 8–10). The amounts of energy dissipated by all the joint models are shown in Figure 14. It must be mentioned that, in the early loading stage, the joints’ cumulative values of energy dissipation were so close to each other. However, when the loading exceeded five cycles, the values of energy dissipation increased considerably. Meanwhile, energy dissipation increased under increasing the loading level (compared to joint under an axial load of 0%) by 200%, 442%, and 583% when exposed to axial load: 25%, 50%, and 75%, respectively. Further, the level of damage reduced the energy dissipation by 13.7% at a 25% damage level and 22.2% at a 50% damage level. On the other hand, FRP composites substantially upgraded the load and displacement by 81% at 0% damage level, 35% at 25% damage level, and 22% at 50% damage level. These values were much better than those of the un-reinforced models, reflecting an improvement in energy dissipation and seismic behavior.

Table 3. Various structural characteristics of the simulated joints.

Specimen	Steel Strain, $\mu\epsilon$	FRP Strain, $\mu\epsilon$	Yield Displacement d_y , mm	Maximum Displacement d_m , mm	Displacement Ductility d_m/d_y	Energy Dissipation, kN.mm
J0FRP0D0	946	----	Not yielded	7.60	NA	165
J25FRP0D0	1419	----	Not yielded	14.90	NA	498
J50FRP0D0	1703	----	2.58	22.29	8.6	918
J75FRP0D0	1797	----	2.12	26.26	12.4	1150
J0FRP0D25	804	----	Not yielded	6.05	NA	115
J25FRP0D25	1239	----	Not yielded	12.28	NA	374
J50FRP0D25	1499	----	Not yielded	17.19	NA	657
J75FRP0D25	1596	----	2.87	20.00	7.0	836
J0FRP0D50	620	----	Not yielded	5.24	NA	75
J25FRP0D50	989	----	Not yielded	10.16	NA	250
J50FRP0D50	1221	----	Not yielded	14.71	NA	481
J75FRP0D50	1376	----	Not yielded	17.65	NA	654
J0FRP1D0	1929	6524	3.03	14.81	4.9	356
J25FRP1D0	3270	10282	2.97	29.18	9.8	1139
J50FRP1D0	4301	12916	2.67	38.04	14.2	1907
J75FRP1D0	4760	13828	2.07	45.73	22.1	2403
J0FRP1D25	1750	5509	4.12	9.82	2.4	211
J25FRP1D25	2816	8917	3.75	19.75	5.3	648
J50FRP1D25	3849	11528	3.61	26.12	7.2	1128
J75FRP1D25	4486	12870	3.06	32.39	10.6	1549
J0FRP1D50	1436	4031	4.71	7.78	1.7	135
J25FRP1D50	2358	7360	4.67	17.28	3.7	503
J50FRP1D50	3243	9617	4.59	22.91	5.0	858
J75FRP1D50	3919	11189	4.05	28.12	6.9	1248

Further, FRP composites absorb energy in an effective manner, decreasing load transfer to other members. The strengthened models' energy dissipation was nearly 4.7 times more than the un-reinforced one, as illustrated in Table 3. The optimum energy dissipation capacity was reached for the strengthened joints with 75% axial load since they had larger displacement and loading capacities. Moreover, Table 3 shows that increasing the loading level increases the energy dissipation capacity; when the axial load was: 25%, 50%, and 75%, the energy dissipation raised by: 185%, 322%, and 413%, respectively. In addition, the damage level decreased the energy dissipation, whereas 25% reduced the dissipated energy by 33%, while 50% reduced dissipation by 51%.

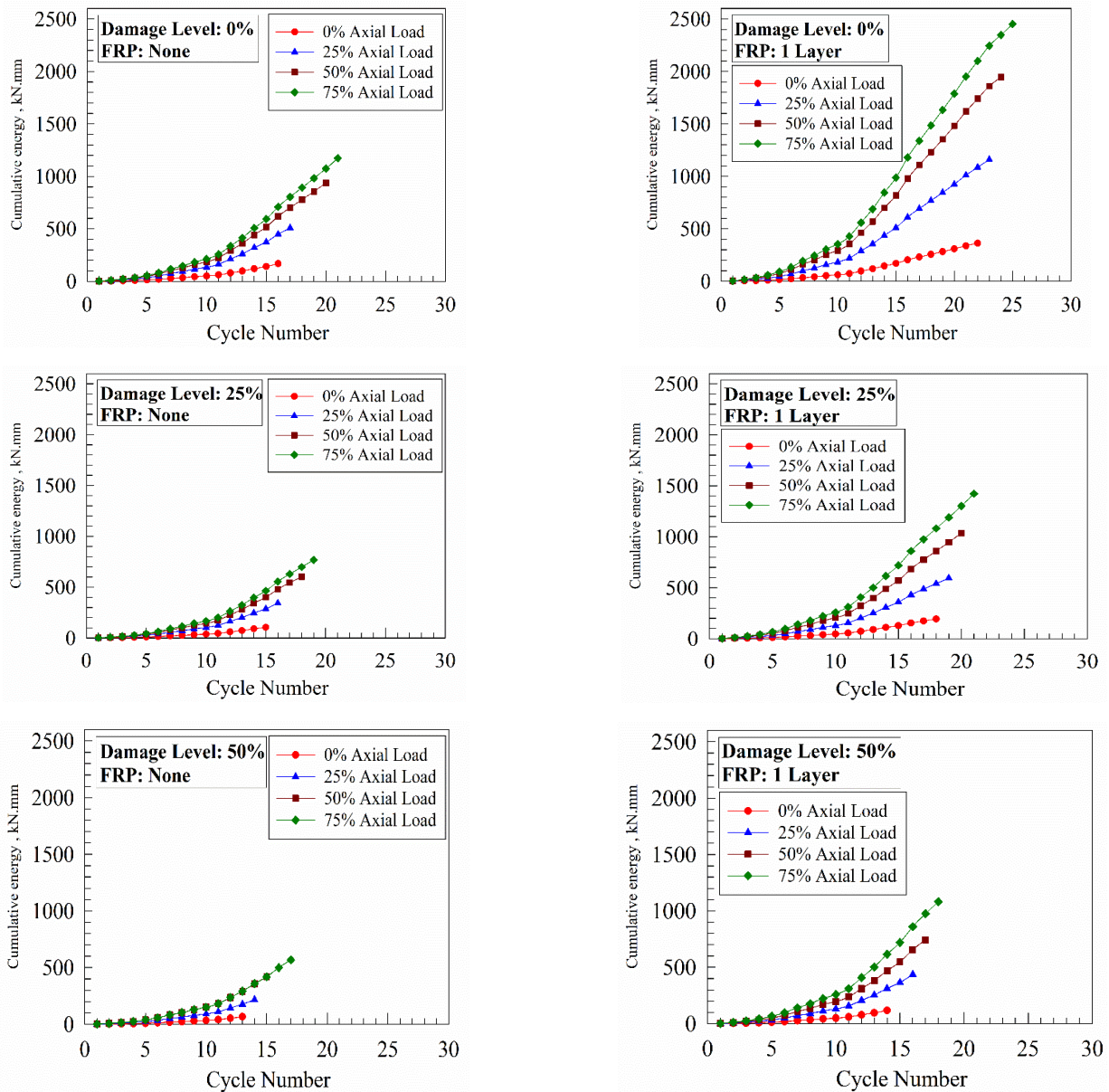


Figure 14. Energy dissipation characteristics.

4.5. Secant Stiffness Degradation and Damping Factor

The resulting degradation in the secant stiffness has been qualitatively measured for the B-C joints in every cycle by plotting every load-displacement loop envelope. The sum of the maximum reached load in pushing-pulling is divided by the resulting displacements representing the slope of the initial line at each cycle. Therefore, the joint’s cyclic stiffness is calculated as per Equation (1) as follows:

$$K_i = \frac{F_i^+ - F_i^-}{D_i^+ - D_i^-} \tag{1}$$

where: F_i^+ and F_i^- are the maximum reached loads in positive and negative directions for each cycle and the corresponding displacements at each cycle i . Figure 15 shows that un-reinforced joints had a drastic degradation in secant stiffness due to the newly initiated cracks at each cycle; that is referred to as the joints’ critical reinforcement details, which reduced the concrete strength, leading to softening. The secant stiffness values’ consistent decrease is pronounced in the strengthened joints because of the perfect confinement

with FRP, as this strengthening method eliminated the emergence of major cracks in the joint area and increased the initial stiffness value. The resulting stiffness degradation is stabilized under the increased loading at each. That is referred to as increasing the axial load, enhancing the column’s compressive stress, and decreasing the diagonal tensile stresses. Moreover, it could be revealed in Figure 15 that stiffness degradation increased minorly under increasing the axial loading level (compared to strengthened joint under 0% of axial load) by 3%, 6%, and 9%, corresponding to an axial loading level of 25%, 50%, and 75%, respectively. In addition, the degradation is reduced by 19% and 38% at 25% and 50% under the various damage levels.

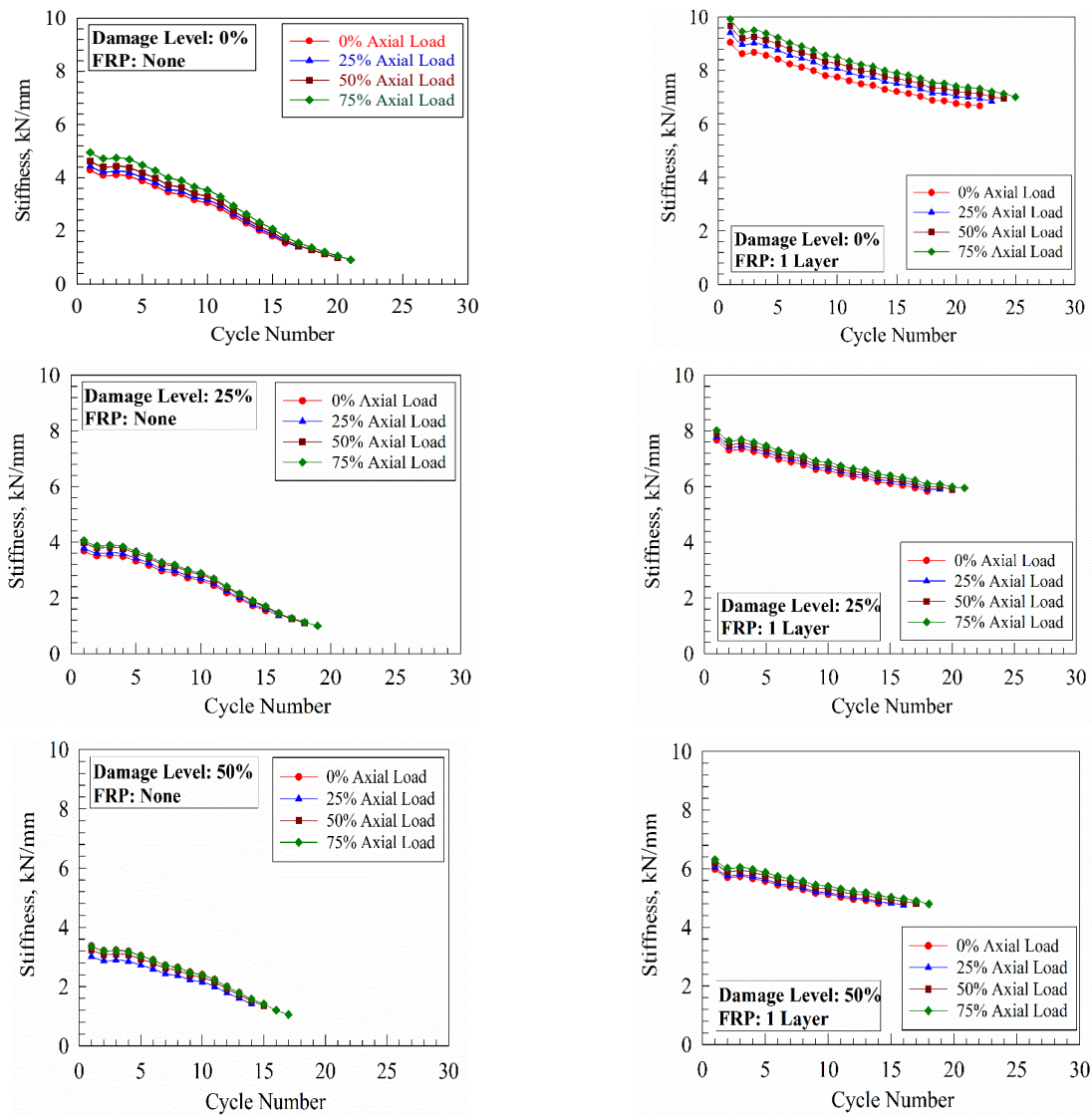


Figure 15. Stiffness degradation behavior.

Meanwhile, dividing the energy dissipation value at the end of each cycle by 2π times the elastic strain energy is generally known as the equivalent damping factor for the hysteresis loops, which is stored within a linear elastic system as per Equation (2) [64]:

$$\tilde{\zeta}_{eqi} = \frac{E_i}{2\pi F_{mi} D_{mi}} \tag{2}$$

where E_i denotes the energy dissipated, F_{mi} is the load value, and D_{mi} is the peak displacements for each loading cycle i .

The calculated damping factor for each cycle is plotted in Figure 16 for all simulated joints. Observing Figure 16 revealed that strengthening the B-C joints with FRP material increases the damping factor significantly compared to the unstrengthened ones. That is interpreted by the fact that the strengthened specimens have enhanced deformability. Meanwhile, the rising damping factor enhanced seismic performance when five loading cycles were reached. However, strengthening the B-C joint with FRP composites has been found to improve the overall performance, including all of its aspects. Consequently, such joints were the best because they were able to convey the failure pattern to the connected area.

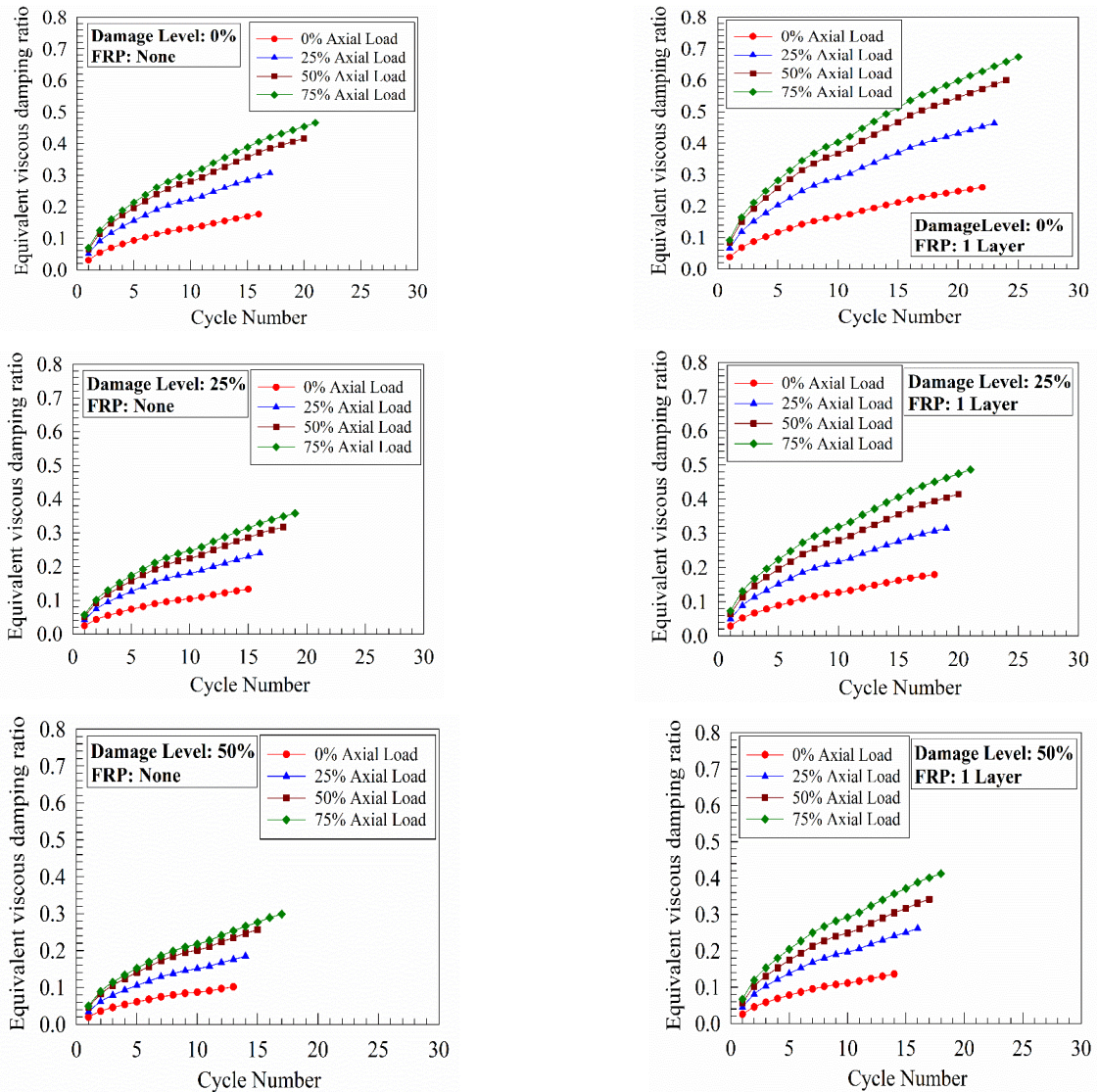


Figure 16. The equivalent damping ratio behavior.

5. Conclusions

The efficiency of utilizing FRP composites in strengthening damaged B-C joints under cyclic loading has been experimentally tested by Shannag and Alhassan [33] and simulated using the NLFEA modeling approach by ANSYS package. Further investigation has been carried out on the effect of the resulting damage level on the concrete compressive strength (0%, 25%, and 50%) and the column’s axial loading (0%, 25%, 50%, and 75%) on the overall performance of the B-C joints and based on the presented results, the following was concluded:

1. Both the column's axial loading and the concrete damage level considerably affect the joint's behavior besides the utilized reinforcement scheme's role in suppressing their effect. However, Stiffness degradation was slightly affected when the axial load was changed but considerably affected the other sensitive performance parameters.
2. Using FRP to reinforce B-C joints externally allows the restoration of strength, and the failure mode of the joint-column area became ductile instead of brittle, making a plastic hinge in the beam only at column axial load levels higher than 25%. Applying axial column loads below 25% enhanced the ultimate axial load and deflection capacities.
3. For FRP-strengthened joints, the energy dissipation is done through the joint before the system de-stabilizes. This is an indicator of the joint's ultimate stress capacity till failure. In contrast, strengthened joint models encountered an overall failure when the beam's maximum capacity was reached, where only 50% of the FRP ultimate strain was reached.
4. Due to the resulting accurate simulation, the behavior of the unstrengthened and FRP-strengthened B-C joints could be effectively predicted using the NLFEA modeling approach. However, the resulting observations help specialized engineers retrofit appropriate B-C joints in already-standing buildings with deficient seismic regions, sparing lives, time, and money.

Author Contributions: Conceptualization, R.A.-R. and N.D.L.; methodology, R.A.-R. and K.A.; formal analysis, R.A.-R. and N.D.L.; investigation, R.A.-R. and O.N.; resources, R.A.-R. and K.A.; data curation, R.A.-R. and K.A.; writing—original draft preparation, R.A.-R. and O.N.; writing—review and editing, M.A., R.A.-R. and K.A.; visualization, R.A.-R., O.N., E.A.V. and A.A.S.; supervision, R.A.-R.; project administration, R.A.-R.; funding acquisition, R.A.-R. All authors have read and agreed to the published version of the manuscript.

Funding: This research was funded by European Union funds, grant number 101007595.

Institutional Review Board Statement: Not applicable.

Informed Consent Statement: Not applicable.

Data Availability Statement: Not applicable.

Acknowledgments: Part of this research was supported by the ADDOPTML (ADDitively Manufactured OPTimized Structures by means of Machine Learning) project (No: 101007595) belonging to the Marie Skłodowska-Curie Actions (MSCA) Research and Innovation Staff Exchange (RISE) H2020-MSCA-RISE-2020. Their support is highly acknowledged. The authors would also like to thank the Jordan University of Science and Technology for its support.

Conflicts of Interest: The authors declare no conflict of interest.

References

1. Akbarzadeh, H.; Maghsoudi, A.A. Experimental and analytical investigation of reinforced high strength concrete continuous beams strengthened with fiber reinforced polymer. *Mater. Des. J.* **2010**, *31*, 1130–1147. [[CrossRef](#)]
2. Liu, Y.; Ma, H.; Li, Z.; Wang, W. Seismic behaviour of full-scale prefabricated RC beam–CFST column joints connected by reinforcement coupling sleeves. *Structures* **2020**, *28*, 2760–2771. [[CrossRef](#)]
3. Bian, J.; Cao, W.; Zhang, Z.; Qiao, Q. Cyclic loading tests of thin-walled square steel tube beam-column joint with different joint details. *Structures* **2020**, *25*, 386–397. [[CrossRef](#)]
4. Attari, N.; Youcef, Y.S.; Amziane, S. Seismic performance of reinforced concrete beam–column joint strengthening by FRP sheets. *Structures* **2019**, *20*, 353–364. [[CrossRef](#)]
5. Najafgholipour, M.A.; Arabi, A.R. A non-linear model to apply beam-column joint shear failure in analysis of RC moment resisting frames. *Structures* **2019**, *22*, 13–27. [[CrossRef](#)]
6. Al-Rousan, R.Z.; Alhassan, M.A.; AlShuqari, E.A. Shear Behavior of plain concrete beams with DSSF strengthened in flexure with anchored CFRP sheets—Effects of DSSF content on the bonding length of CFRP sheets. *Case Stud. Constr. Mater.* **2018**, *9*, e195.
7. Al-Rousan, R.Z. Shear behavior of RC beams externally strengthened and anchored with CFRP composites. *Struct. Eng. Mech.* **2017**, *64*, 447–456.
8. Al-Rousan, R.Z.; Issa, M.A. The effect of beam depth on the shear behavior of reinforced concrete beams externally strengthened with carbon fiber–reinforced polymer composites. *Adv. Struct. Eng.* **2016**, *19*, 1769–1779. [[CrossRef](#)]

9. Alhassan, M.A.; Al-Rousan, R.Z.; Abu-Elhija, A.M. Anchoring holes configured to enhance the bond-slip behavior between CFRP composites and concrete. *Constr. Build. Mater.* **2020**, *250*, 11890. [[CrossRef](#)]
10. Al-Rousan, R.Z.; AL-Tahat, M.F. Consequence of anchoring holes technique on the bond behavior between CFRP composites and heat-damaged concrete. *Structures* **2020**, *27*, 1903–1918. [[CrossRef](#)]
11. Monteiro, P.J.M.; Kurtis, K.E. Time to failure for concrete exposed to severe sulfate attack. *Cem. Concr. Res.* **2003**, *33*, 987–993. [[CrossRef](#)]
12. Al-Rousan, R.Z.; AL-Tahat, M.F. Consequence of surface preparation techniques on the bond behavior between concrete and CFRP composites. *Constr. Build. Mater.* **2019**, *212*, 62–374. [[CrossRef](#)]
13. Al-Rousan, R.; Issa, M. Fatigue performance of reinforced concrete beams strengthened with CFRP sheets. *Constr. Build. Mater.* **2011**, *25*, 3520–3529. [[CrossRef](#)]
14. Al-Rousan, R.Z.; Issa, M.A. Flexural behavior of RC beams externally strengthened with CFRP composites exposed to severe environment conditions. *KSCE J. Civ. Eng.* **2017**, *21*, 2300–2309. [[CrossRef](#)]
15. Al-Rousan, R.Z.; Haddad, R.H.; Swesi, A.O. Repair of shear-deficient normal weight concrete beams damaged by thermal shock using advanced composite materials. *Compos. Part B Eng.* **2015**, *70*, 20–34. [[CrossRef](#)]
16. Hekal, E.E.; Kishar, E.; Mostafa, H. Magnesium sulfate attack on hardened cement pastes under different circumstances. *Cem. Concr. Res.* **2002**, *32*, 1421–1427. [[CrossRef](#)]
17. Al-Dulajjan, S.U.; Mashlehuiddin, M.; Al-Zahrán, M.M.; Sharif, A.M.; Shameen, M.; Ibrahim, M. Sulfate resistance of plain and blended cements exposed to varying concentration of sodium sulfate. *Cem. Concr. Compos.* **2003**, *25*, 429–437. [[CrossRef](#)]
18. Qaderi, S.; Ebrahimi, F.; Vinyas, M. Dynamic analysis of multi-layered composite beams reinforced with graphene platelets resting on two-parameter viscoelastic foundation. *Eur. Phys. J. Plus* **2019**, *134*, 1–11. [[CrossRef](#)]
19. Shariati, A.; Qaderi, S.; Ebrahimi, F.; Toghróli, A. On buckling characteristics of polymer composite plates reinforced with graphene platelets. *Eng. Comput.* **2020**, *10*, 1–2. [[CrossRef](#)]
20. Lee, S.T.; Moon, H.Y.; Hooton, R.D.; Kim, J.P. Effect of solution concentrations and replacement levels of metakaolin on the resistance of mortar exposed to magnesium sulfate solution. *Cem. Concr. Res.* **2005**, *35*, 1314–1323. [[CrossRef](#)]
21. Zia, P.; Ahmad, S.H.; Garg, R.K.; Hanes, K.M. Flexural and shear behavior of concrete beams reinforced with 3-D continuous carbon fiber fabric. *Concr. Int.* **1992**, *14*, 48–52.
22. Ehsani, M.R.; Wight, J.K. Exterior reinforced concrete beam-to-column connections subjected to earthquake-type loading. *ACI J.* **1985**, *82*, 492–499.
23. Marthong, C.; Sangma, A.S.; Choudhury, S.A.; Pyrbot, R.N.; Tron, S.L.; Mawroh, L.; Bharti, G.S. Structural Behavior of Recycled Aggregate Concrete Beam-Column Connection in Presence of Micro Concrete at Joint Region. *Structures* **2017**, *11*, 243–251. [[CrossRef](#)]
24. Masi, A.; Santarsiero, G.; Moroni, C.; Nigro, D.; Dolce, M.; Russo, G.; Pauletta, M.; Realfonzo, R.; Faella, C.; Lignola, G.P.; et al. Behaviour and strengthening of RC beam-column joints: Experimental Program and first results of the research activity in the framework of DPC- Reluis Project (Research Line 2). In Proceedings of the 14th World Conference on Earthquake Engineering, Beijing, China, 12–17 October 2008.
25. Alhassan, M.A.; Al-Rousan, R.Z.; Amaireh, L.K.; Barfed, M.H. Nonlinear Finite Element Analysis of B-C Connections: Influence of the Column Axial Load, Jacket Thickness, and Fiber Dosage. *Structures* **2018**, *16*, 50–62. [[CrossRef](#)]
26. Shiohar, H. Reinforced concrete beam-column joints: An overlooked failure mechanism. *ACI Struct. J.* **2012**, *109*, 65–74.
27. Yang, J.; Sheehan, T.; Dai, X.; Lam, D. Structural Behaviour of Beam to Concrete-filled Elliptical Steel Tubular Column Connections. *Structures* **2017**, *9*, 41–52. [[CrossRef](#)]
28. Démonceau, J.-F.; Ciutina, A. Characterisation of Beam-to-column Steel-concrete Composite Joints Beyond Current Eurocode Provisions. *Structures* **2019**, *21*, 167–175. [[CrossRef](#)]
29. Roy, B.; Laskar, A.I. Cyclic Performance of Beam-Column Subassemblies with Construction Joint in Column Retrofitted with GFRP. *Structures* **2018**, *14*, 290–300. [[CrossRef](#)]
30. Xian, G.; Guo, R.; Li, C.; Wang, Y. Mechanical performance evolution and life prediction of prestressed cfrp plate exposed to hygrothermal and freeze-thaw environments. *Compos. Struct.* **2022**, *293*, 115719. [[CrossRef](#)]
31. Li, C.; Guo, R.; Xian, G.; Li, H. Effects of elevated temperature, hydraulic pressure and fatigue loading on the property evolution of a carbon/glass fiber hybrid rod. *Polym. Test.* **2020**, *90*, 106761. [[CrossRef](#)]
32. Elmesalami, N.; Abed, F.; Refai, A.E. Concrete columns reinforced with GFRP and BFRP bars under concentric and eccentric loads: Experimental testing and analytical investigation. *J. Compos. Constr.* **2021**, *25*, 04021003. [[CrossRef](#)]
33. Al-shannag, M.; Alhassan, M. Upgrading the Structural Seismic Behavior of Gld-Frames with HPFRC-Jackets. *ACI Struct. J.* **2005**, *102*, 131–138.
34. Realfonzo, R.; Napoli, A.; Pinilla, J.G. Cyclic behavior of RC beam-column joints strengthened with FRP systems. *Constr. Build. Mater.* **2014**, *54*, 282–297. [[CrossRef](#)]
35. Engindeniz, M.; Kahn, L.F.; Zureick, A.H. Repair and strengthening of reinforced concrete beam-column joints: State of the art. *ACI Struct. J.* **2005**, *102*, 1–14.
36. Beschi, C.; Meda, A.; Riva, P. Column and joint retrofitting with high performance fiber reinforced concrete jacketing. *J. Earthq. Eng.* **2011**, *15*, 989–1014. [[CrossRef](#)]

37. Bousselham, A. State of research on seismic retrofit of RC beam-column joints with externally bonded FRP. *J. Compos. Construct.* **2010**, *14*, 49–61. [[CrossRef](#)]
38. El-Amoury, T.; Ghobarah, A. Seismic rehabilitation of beam–column joint using GFRP sheets. *Eng. Struct.* **2002**, *24*, 1397–1407. [[CrossRef](#)]
39. Ghobarah, A.; El-Amoury, T. Seismic rehabilitation of deficient exterior concrete frame joints. *J. Compos. Construct.* **2005**, *9*, 408–416. [[CrossRef](#)]
40. Sasmal, S.; Ramanjaneyulu, K.; Novák, B.; Srinivas, V.; Kumar, K.S.; Korkowski, C.; Roehmb, C.; Lakshmanana, N.; Iyera, N.R. Seismic retrofitting of non-ductile beam-column sub-assembly using FRP wrapping and steel plate jacketing. *Construct. Build. Mater.* **2011**, *25*, 175–182. [[CrossRef](#)]
41. Antonopoulos, C.P.; Triantafillou, T.C. Experimental investigation of FRP- strengthened RC beam-column joints. *J. Compos. Construct.* **2003**, *7*, 39–49. [[CrossRef](#)]
42. Al-Salloum, Y.A.; Siddiqui, N.A.; Elsanadedy, H.M.; Abadel, A.A.; Aqel, M.A. Textile- reinforced mortar versus FRP as strengthening material for seismically deficient RC beam-column joints. *J. Compos. Construct.* **2011**, *15*, 920–933. [[CrossRef](#)]
43. Hamid, S.; Mohd, Z.J.; Mahdi, S. Numerical investigation on exterior reinforced concrete Beam-Column joint strengthened by composite fiber reinforced polymer (CFRP). *Int. J. Phys. Sci.* **2011**, *6*, 6572–6579.
44. Del Vecchio, C.; Di Ludovico, M.; Prota, A.; Manfredi, G. Modelling beam-column joints and FRP strengthening in the seismic performance assessment of RC existing frames. *Compos. Struct.* **2016**, *142*, 107–116. [[CrossRef](#)]
45. Mosallam, A.; Allam, K.; Salama, M. Analytical and numerical modeling of RC beam-column joints retrofitted with FRP laminates and hybrid composite connectors. *Compos. Struct.* **2019**, *214*, 486–503. [[CrossRef](#)]
46. Eligehausen, R.; Genesio, G.; Ozbolt, J.; Pampanin, S. 3D analysis of seismic response of RC beam-column exterior joints before and after retrofit. In *Concrete Repair, Rehabilitation and Retrofitting II*; CRC Press: Boca Raton, FL, USA, 2008; pp. 407–408.
47. Sasmal, S. Performance Evaluation and Strengthening of Deficient Beam-Column Sub-Assemblages under Cyclic Loading. Ph.D. Thesis, Universität Stuttgart, Stuttgart, Germany, 2009; 173p.
48. Venkatesan, B.; Ilangoan, R.; Jayabalan, P.; Mahendran, N.; Sakthieswaran, N. Finite element analysis (FEA) for the beam-column joint subjected to cyclic loading was performed using ANSYS. *Circuits Syst.* **2016**, *7*, 1581–1597. [[CrossRef](#)]
49. Sasmal, S.; Nath, D. Evaluation of performance of non-invasive upgrade strategy for beam–column sub-assemblages of poorly designed structures under seismic type loading. *Earthq. Eng. Struct. Dyn.* **2016**, *45*, 1817–1835. [[CrossRef](#)]
50. Li, B. Seismic Performance of Reinforced Concrete Beam-Column Joints Strengthened by Ferrocement Jackets. Ph.D. Thesis, The Hong Polytechnic University, Hong Kong, China, 2014; 278p.
51. Sasmal, S.; Ramanjaneyulu, K.; Novák, B.; Lakshmanan, N. Analytical and experimental investigations on seismic performance of exterior beam–column sub-assemblages of existing RC-framed building. *Earthq. Eng. Struct. Dyn.* **2013**, *42*, 1785–1805. [[CrossRef](#)]
52. Ibrahim, G. Shaabana and Mohamed Said. Finite element modeling of exterior beam-column joints strengthened by ferrocement under cyclic loading. *Case Stud. Constr. Mater.* **2018**, *8*, 333–346.
53. Al-Rousan, R.; Haddad, R.; Al-Sa’di, K. Effect of Sulfates on bond behavior between carbon fiber reinforced polymer sheets and concrete. *Mater. Des. J.* **2013**, *43*, 237–248. [[CrossRef](#)]
54. ANSYS. *ANSYS User’s Manual Revision 16.0*; ANSYS, Inc.: Kanonsburg, PA, USA, 2015.
55. ACI Committee 318. *Building Code Requirements for Reinforced Concrete (ACI 318-08) and Commentary (318R-08)*; American Concrete Institute: Farmington Hills, MI, USA, 2008; p. 443.
56. Kent, D.C.; Park, R. Flexural members with confined concrete. *J. Struct. Div.* **1971**, *7*, 85–94. [[CrossRef](#)]
57. Khaled, A.K.; Mosallam, A.S.; Salama, M.A. Experimental evaluation of seismic performance of interior RC beam-column joints strengthened with FRP composites. *Eng. Struct.* **2019**, *196*, 109308.
58. ASCE Task Committee on Concrete and Masonry Structure. *State of the Art Report on Finite Element Analysis of Reinforced Concrete*; ASCE: Reston, VA, USA, 1982.
59. ACI Committee 318. *Building Code Requirements for Structural Concrete (ACI 318-014) and Commentary (ACI 318R-14)*; American Concrete Institute: Farmington Hills, MI, USA, 2014.
60. Hemmaty, Y. Modeling of the shear force transferred between cracks in reinforced and fiber reinforced concrete structures. In *Proceedings of the ANSYS Conference, Pittsburgh, PA, USA, 30 September 1998*; Volume 1, pp. 1–13.
61. Huyse, L.; Hemmaty, Y.; Vandewalle, L. Finite element modeling of fiber reinforced concrete beams. In *Proceedings of the ANSYS Conference, Pittsburgh, PA, USA, 30 September 1994*; Volume 2.
62. Haddad, R.H.; Al-Rousan, R.Z.; Al-Sedyiri, B.K. Repair of shear-deficient and sulfate-damaged reinforced concrete beams using FRP composites. *Eng. Struct. J.* **2013**, *56*, 228–238. [[CrossRef](#)]
63. Kabir, M.Z.; Hojatkashani, A. A comparison between finite element and analytical solutions of interfacial stress distribution in a RC beam retrofitted with FRP composites. *Int. J. Sci. Technol.* **2008**, *19*, 55–63.
64. Priestley, M.; Seible, F.; Calvi, G.M. *Seismic Design and Retrofit of Bridges*; John Wiley & Sons: New York, NY, USA, 1996.

Disclaimer/Publisher’s Note: The statements, opinions and data contained in all publications are solely those of the individual author(s) and contributor(s) and not of MDPI and/or the editor(s). MDPI and/or the editor(s) disclaim responsibility for any injury to people or property resulting from any ideas, methods, instructions or products referred to in the content.